RESEARCH

Optimal thickness and annealing temperature for enhancement of structural, optical, and photocatalytic properties of ZnO thin films

A. Abdel-Galil[1] · Mai S. A. Hussien[2,3] · M. R. Balboul[1]

Abstract

Thin films of ZnO, with distinct thicknesses, were deposited on soda-lime glass substrates by sol–gel spin-coating as a cost-effective method without any evacuation facilities. The nanocrystalline structure of the deposited films was indexed by the atomic force microscope and X-ray diffraction techniques. The average grain size increases with the increase of the film thickness and annealing temperature. The energy-dispersive X-ray technique has been used to check the atomic ratios of Zn and O with the film thickness and heat treatment for homogeneous ZnO films. ZnO films show elevated transmission in the visible spectrum as a transparent semiconductor material. Optical constants, like absorption coefficient, optical band gap, and refractive index, were obtained by the Swanepoel method. All thin film samples were applied for photodegradation of reactive orange 96 (RO96) to evaluate the effect of thickness and annealing temperature on the ZnO film's photocatalytic activity. ZnO 4L (400 °C, 3 h) film possesses the highest rate of photodegradation about 0.1 min^{-1} for RO96 with high stability and reusability.

Keywords Crystal structure · Optical constants · X-ray diffraction pattern · Dispersion parameters · ZnO · Photocatalysis

Introduction

Zinc oxide (ZnO) has elevated transmittance, excellent electric conductivity, and a broad optical bandgap with high exciton-binding energy of 60 meV at room temperature as a semiconductor material [1, 2]. ZnO as a metal oxide belongs to the II–VI group, characterized by its chemical and physical stability, abundance, economical feasibility, and environment friendly. Also, due to its characteristic optical band gap and good optical transmittance, ZnO can be used for a lot of applications such as dye-sensitized solar hybrid cells [3, 4], a cathode buffer layer, a transparent solar cell window electrode [5, 6], and gas sensor [7]. The stability of ZnO against photo-corrosion and photo-chemical characteristics makes it a potential candidate for solar power conversion as a semi-conductive material [8, 9]. Also, it has been considered as a promising material for water and wastes treatment according to its high activity, environment-friendly merit, and low price [10–12]. ZnO as explained in previous works can decay organic dyes such as methylene blue, rhodamine B, methyl red, and methyl orange under UV irradiation [13–16]. The particle sizes, the concentration of oxygen defects, and surface area have the most attention to promote the photocatalytic activity of ZnO. The surface defects of ZnO thin films are a very remarkable factor affecting its photocatalytic activity [17]. Most of the technological applications depend on the thin films of ZnO, however, the use of nanoparticles powder is not the optimal solution for the different applications. Thin films of ZnO would be more appropriate as a photocatalyst especially in the water treatment because the photocatalytic material remains fixed and can be removed easily by redrawing the film from the treated water. So, the thin films of ZnO can be considered as promising structures for photocatalytic applications [10, 18] because of many factors such as small size, lightweight, stability, reusability, and ability to configure in different frameworks compared to their nanoparticles counterparts. The

✉ A. Abdel-Galil
  ahgalil75@gmail.com

[1] Solid State Physics and Accelerators Department, National Centre for Radiation Research and Technology (NCRRT), Egyptian Atomic Energy Authority (EAEA), Nasr City, Cairo, Egypt

[2] Chemistry Department, Faculty of Education, Ain Shams University, Roxy, Cairo 11757, Egypt

[3] Nanoscience Laboratory for Environmental and Bio-Medical Applications (NLEBA), Faculty of Education, Ain Shams University, Roxy, Cairo 11757, Egypt

physical and chemical properties of ZnO can be tailored for different applications by a variety of processing techniques, such as synthesis procedures, doping mechanism optimization, introduction of impurities, controlling the microstructure, and thickness of the films. Recently, the development of ZnO thin films and powders in nano-scale has led to more efficient electronic and optoelectronic devices. ZnO thin films can be prepared using various methods, such as magnetron sputtering technique [19], molecular beam epitaxy (MBE) [20], metal organic chemical vapor deposition (MOCVD) [21], pulsed laser deposition (PLD) [22], spray pyrolysis [10, 23], ultrasonic spray [24], and sol–gel process [25]. However, the sol–gel spin-coating method is more convenient among the other methods, because of low-cost, accurate compositional control, low crystallization temperature, homogeneity at the molecular level, and easy reproducibility. In the present work, ZnO thin films of distinct thicknesses were deposited by the non-vacuum cost-effective sol gel spin-coating technology on soda-lime glass (SLG) substrates at room temperature. The ZnO films with various thicknesses were used as-deposited (fresh) and annealed at 400 °C for 3 h for different characterizations. The X-ray diffraction technique was used to recognize the crystal structure of the deposited ZnO films of distinct thicknesses. The optical characteristics such as optical band gap, absorption coefficient, and refractive index in the UV–VIS-IR range have been determined. Besides, the photocatalytic activity of ZnO thin films and the effect of the film thickness for the photodegradation of Reactive Orange 96 (RO96) under UV irradiation have been evaluated.

Experimental

Materials and preparation

Zinc acetate dihydrate for the ZnO precursor was first dissolved into 2-methoxy ethanol and monoethanolamine (MEA) solution blend, without further heating with 1 M zinc acetate concentration and a molar ratio of 1.0. The mixture has been then stirred at 60 °C for 60 min to produce a transparent and homogeneous solution. The ZnO precursor solution can be left for 48 h, at room temperature before the spin-coating process to achieve the gelation process. It should be noted that when aging has surpassed 48 h, small particles have begun to precipitate, thus affecting the quality of the film made from this precursor solution. ZnO thin films were deposited on soda-lime glass (SLG) as transparent substrates through the spin coater (VTC-100 model vacuum) in two steps; with 500 rpm for 5 s and 3000 rpm for 30 s. In order to evaporate the solvent and remove the organic residue, the synthesized ZnO thin films were dried at 250 °C for 10 min by the hot plate in the air. The procedures from coating to drying have been repeated to achieve ZnO films with thicknesses of one, two, three, four,

and five layers (1L, 2L, 3L, 4L, 5L). The as-deposited (fresh) furthermore the annealed at 400 °C for 3 h (400 °C, 3 h) ZnO films with the five thicknesses (1L, 2L, 3L, 4L, 5L) have been utilized for the characterizations. Before ZnO thin films are deposited, SLG glass substrates have been ultrasonically washed (Bransonic 1210, USA) for 15 min, consecutively, by acetone, ethanol, and distilled water.

Photocatalytic degradation

Reactive Orange 96 (RO96) aqueous solution was used for the photodegradation study. ZnO thin films as a catalyst suspended in 200 ml of RO96 solution and then the solution with ZnO films were placed in the photoreactor under the illumination of 6-W Hg lamps (254 nm) to achieve a radiation flux of 20 $MWcm^2$ of UV irradiation. The UV radiation flux was measured at ambient temperature by using a Digital UVX36 luxmeter. The thin films were withdrawn, and subsequently, the concentration of the dye aqueous solution was evaluated by measuring the absorbance of the dye solution at different intervals of time under the UV irradiation.

Characterization of nanostructured ZnO thin films

The composition stoichiometry of ZnO fresh and annealed (400 °C, 3 h) thin films of different thicknesses was investigated by energy-dispersive X-ray (EDX) spectroscopy using a scanning electron microscope (Jeol JSM-5400 with Oxford link Isis detector) operating at an accelerating voltage of 30 keV. The average grain size, surface morphology, and roughness shape parameters of ZnO thin films have been investigated through the atomic force microscope (AFM) images using Agilent Instruments 5500. Surface morphology of the deposited thin films also has been checked by scanning electron microscope, ZEISS-EVO 15-UK. X-ray diffraction (XRD, Shimadzu XD-6000) operates with 40 keV and 30 mA with Cuk_α wavelength radiation $\lambda = 1.5418$ Å has been employed to recognize the crystal structure of ZnO thin films. The absorbance and transmittance spectra of the spin-coated ZnO thin films, at the normal incidence of light, have been measured by utilizing a double beam computer-controlled spectrophotometer (JASCO V-670 UV/VIS/NIR) in the wavelength range of 190 to 2500 nm.

Results and discussion

Structural study of nanostructured ZnO thin films

The average grain size, roughness, and shape parameters for fresh and annealed (400 °C, 3 h) ZnO (2L, 3L, and 4L) films have been examined through high-resolution AFM images as shown in Fig. 1a, b, c, d, e, f respectively. The surface
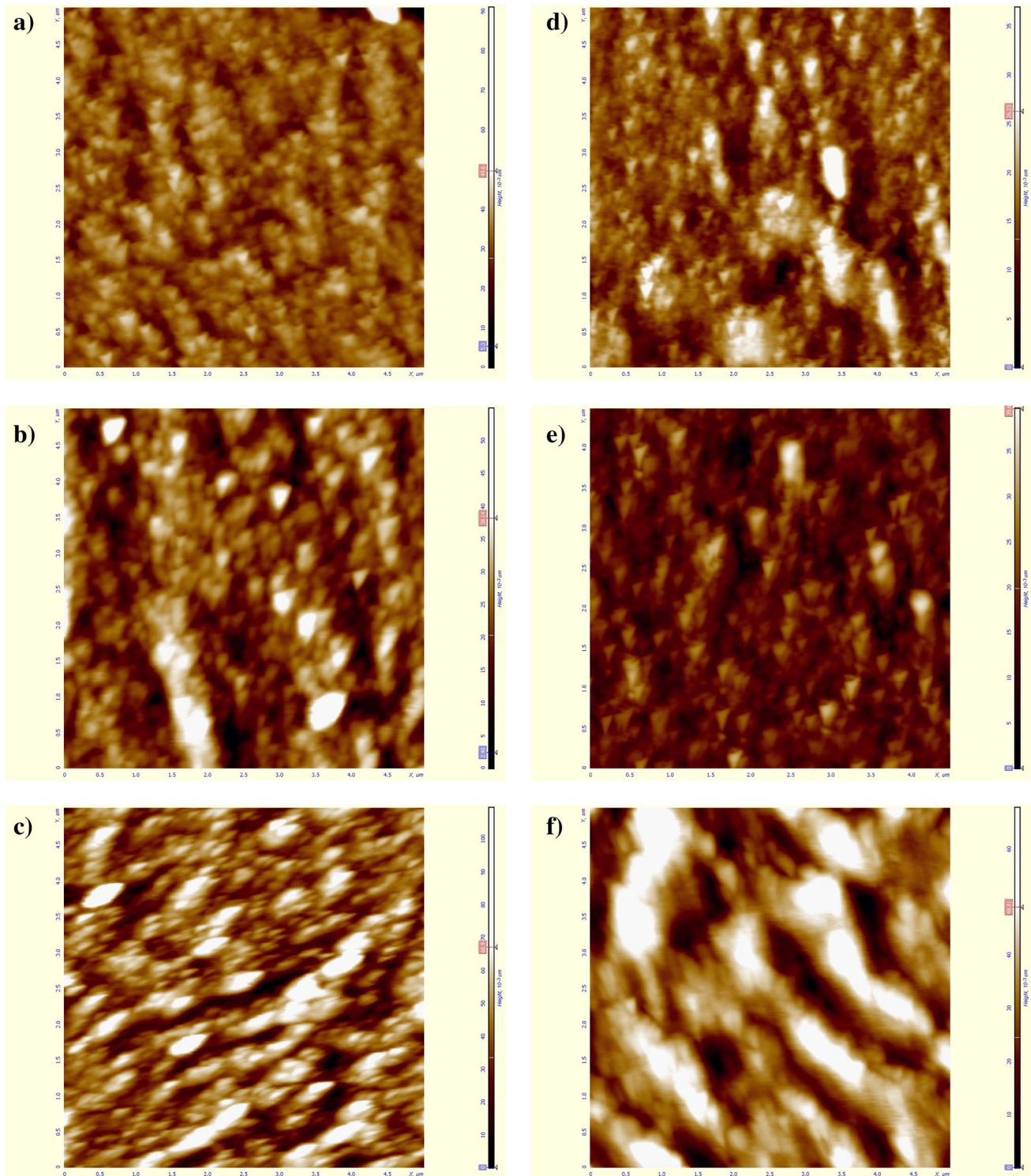
Fig. 1 Surface morphology of ZnO fresh **a** 2L, **b** 3L, **c** 4L, and annealed (400 °C, 3 h) **d** 2L, **e** 3L, **f** 4L thin films

morphology and the average grain size of the films under investigation are found to be obviously dependent on the thickness of the film and the annealing temperature. As shown in Fig. 1a, b, c, d, e, f the substrates have been well covered by compact and tightly linked crystalline grains with symmetrical shapes. The size and the shape of grains depend on the thickness and the annealing temperature of the film. Furthermore, ZnO films of all thicknesses exhibit strong adhesion with smooth

distribution over the glass substrates. Tables 1 and 2 reveal the values of average grain size (D_A), roughness parameters (average roughness, R_a and root mean square roughness, R_q), and shape parameters (roughness skewness, R_{sk}, and roughness kurtosis, R_{ku}) for fresh and annealed ZnO thin films, respectively. As observed from those tables, with the annealing temperature (400 °C, 3 h) and the increase of the film thickness, the average grain size (D_A) increases. Also, R_q (the square root of the distribution of surface height) and R_a (the mean height) increase with the film thickness and with the annealing temperature in the same manner. These results can be explained as the follows: through the annealing process, the high temperature can stimulate the grain boundaries to migrate and cause the coalescence of more grains, hence the rise of the average grain size and surface roughness [26–28]. The positive values of R_{sk} for all thicknesses of ZnO fresh and annealed films show that the peaks are dominant in the film surface. The values of R_{ku} which are less than 3 in the case of ZnO (2L & 4L) fresh films and 4L annealed film mean broad low peaks and valleys (bumpy surface); while with the values of R_{ku} greater than 3, the surface consists of sharp high peaks and scratches (spiky surface) as in the case of 3L fresh film and (2L & 3L) annealed films.

SEM images of the deposited films (a) 4L fresh, (b) 4L annealed at 400 °C, (c) 5L fresh, and (d) 5L annealed at 400 °C have been performed and represented in Fig. 2a, b, c, d. As shown in that figure, SEM images confirm that thin film surfaces consist of compact and tightly linked crystalline grains with spherical shapes well cover the glass substrates with strong adhesion. Also, as we note from the figure, the crystallites' size increases with the film thickness and the annealing temperature. The EDX point assessment as shown in Table 3 allows testing of the atomic proportions of the constituents (Zn and O) and the uniformity of the synthesized films. As shown in that table, the increase of the film thickness increases the Zn ratios and decreases the percentage of oxygen. While the oxygen ratio increased for

Table 1 AFM average grain size, roughness, and shape parameters for ZnO fresh (2L, 3L, and 4L) thin films

ZnO	D_A (nm)	R_a (nm)	R_q (nm)	R_{sk} (nm)	R_{ku} (nm)
2L	95.23	23.50	29.66	0.345	2.970
3L	110.50	45.80	62.95	1.270	3.960
4L	122.20	52.49	63.45	0.708	2.663

Table 2 AFM average grain size, roughness, and shape parameters for ZnO annealed (400 °C, 3 h) (2L, 3L, and 4L) thin films

ZnO	D_A(nm)	R_a (nm)	R_q (nm)	R_{sk} (nm)	R_{ku} (nm)
2L	130.83	48.25	63.66	1.09	3.381
3L	150.50	11.49	17.45	2.439	7.730
4L	180.20	72.80	83.95	0.356	1.959

the annealed ZnO films, where the charged oxygen-related species are adsorbed on the crystalline film and the structure defects have been treated. For ZnO fresh film with 4L of thickness, the optimal Zn and O ratios can be achieved as a stoichiometric compound of ZnO. At 400 °C for 3 h, the Zn and O ratios, in ZnO (4L) film, can be improved to obtain the more stoichiometric compound of ZnO where the oxygen vacancies can be treated.

Figure 3a, b illustrate the X-ray diffraction patterns of the fresh and annealed ZnO films with different thicknesses. In accordance with the hexagonal wurtzite structure (JCPDS spectrum card No. 36–1451), ZnO films exhibit preferential orientation along (002) plane for all the deposited films. With the annealing temperature (400 °C, 3 h), and increasing the film thickness, the other two characteristic peaks (100) and (101) begin to appear. Through the thermal treatment (400 °C, 3 h) and film thickness, the intensity of the three distinctive peaks of the films improved. The average grain size D for ZnO (fresh & annealed) films at (002) plane can be evaluated through the Scherrer formula [29]:

$$D = \frac{0.94\lambda}{\beta_{2\theta}\cos\theta}, \tag{1}$$

where the wavelength of the used X-ray is λ and the full width at half maximum is $\beta_{2\theta}$.

The lattice misfit, which is the main source for the microstrain and broadening of the diffracted peaks, depends upon the deposition conditions. The micro-strain ε for ZnO thin films understudy can be computed by the relation:

$$\varepsilon = \frac{1}{4}\beta_{2\theta}\cos\theta, \tag{2}$$

The dislocation density δ as line defects in the ZnO fresh and annealed films can be estimated by using Williamson and Smallman's relation [30]:

$$\delta = \frac{1}{D^2} \tag{3}$$

The average grain size, micro-strain, and dislocation density values for all ZnO thin films under study are represented in Table 4. The grain size for ZnO thin film samples are in the nano-scale for all films and its value increases with the film thickness and annealing temperature. As we note from Tables 1, 2, and 4, the average grain size obtained from the AFM image analysis has larger values than those of the XRD results. This difference in the grain size can be explained according to S. Gürakar et.al [31] where they stated that the large crystallites which appear in the AFM images can be considered as a direct result of the agglomerations of the nanocrystalline ZnO grains in the film surface, while the XRD technique can record the signals from crystals on the surface and inside the films, owing to the good penetration
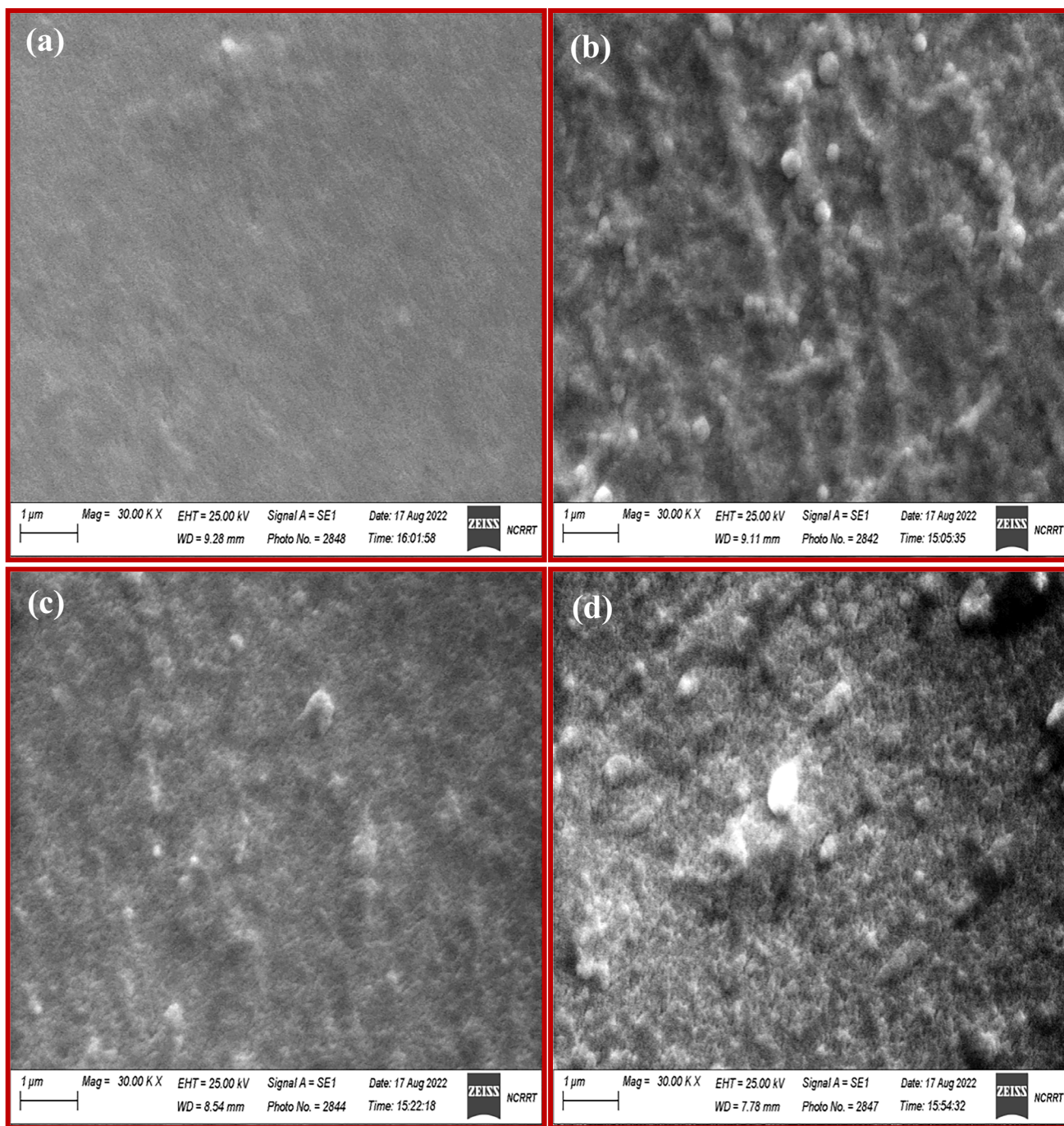
Fig. 2 SEM images of **a** 4L fresh, **b** 4L annealed (400 °C, 3 h) **c** 5L fresh, and **d** 5L annealed (400 °C, 3 h) thin films

depth of the X-ray within the film. So, XRD result can give accurate values of the average grain size than that of AFM.

For the annealed (400 °C, 3 h) ZnO films and with the increase of film thickness, the micro-strain and dislocation

ZnO	Fresh					400 °C, 3 h				
	1L	2L	3L	4L	5L	1L	2L	3L	4L	5L
Zn (atomic %)	15.14	28.73	40.76	50.31	57.38	13.46	25.34	37.32	48.25	55.43
O (atomic %)	84.86	71.27	59.24	49.69	42.62	86.54	74.66	62.68	51.75	44.57

Table 3 EDX data (atomic %) for ZnO (fresh & annealed) thin films

Fig. 3 X-ray diffractions for ZnO **a** fresh and **b** annealed (400 °C, 3 h) thin films
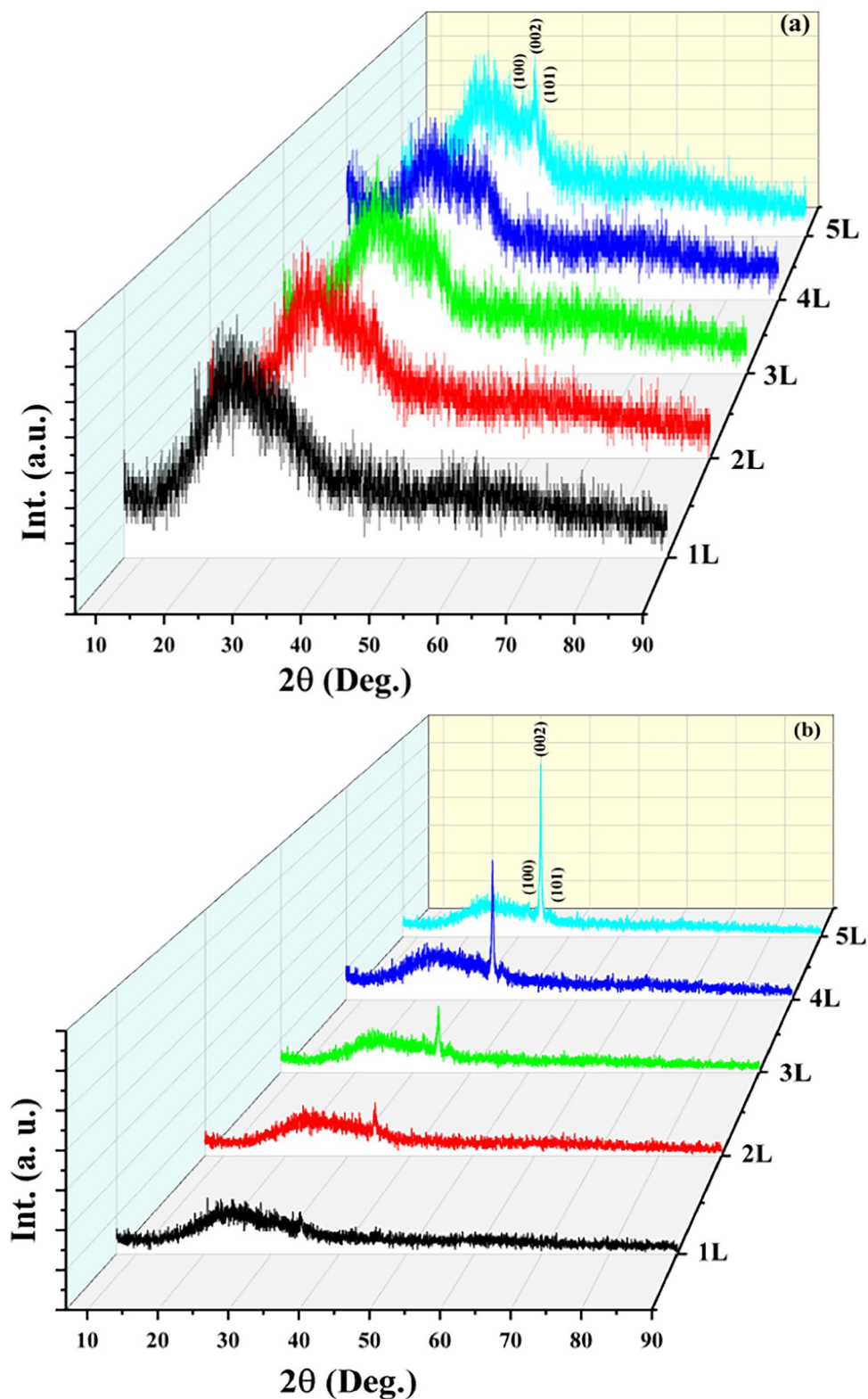
density as structural defects reduce. This means that the heat treatment at 400 °C for 3 h enhances the crystal structure and reduces the defect density in ZnO thin films where the struc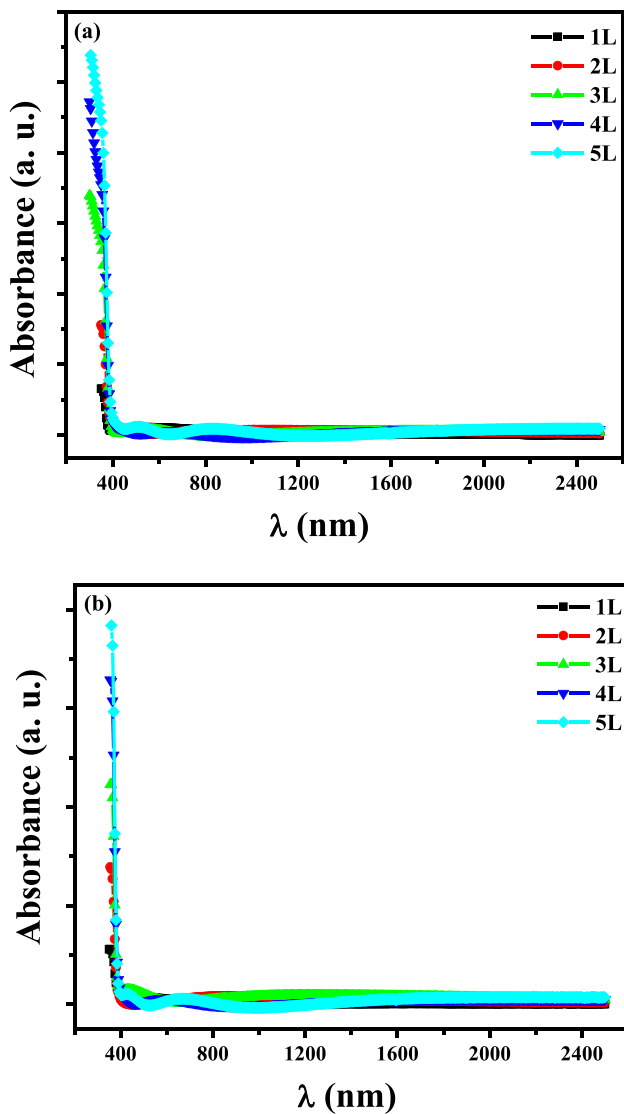tural defects can act as recombination centers for the photogenerated electron–hole pairs in the photocatalytic and optoelectronic applications. These results confirm the applicability of the sol–gel spin-coating ZnO films as efficient photocatalysts in wastewater purification.

Table 4 Structure parameters for ZnO (fresh & annealed) thin films

ZnO	Fresh			400 °C, 3 h		
	D (nm)	$\varepsilon \times 10^{-3}$	$\delta \times 10^{12}$ (lin cm^{-2})	D (nm)	$\varepsilon \times 10^{-3}$	$\delta \times 10^{11}$ (lin cm^{-2})
1L	5.26	6.59	3.62	12.58	2.76	6.32
2L	5.83	5.95	2.95	19.29	1.80	2.69
3L	6.71	5.17	2.22	25.21	1.38	1.57
4L	7.95	4.36	1.58	27.18	1.28	1.35
5L	8.18	4.24	1.49	29.73	1.17	1.13

Optical properties of nanostructured ZnO thin films

The optical absorbance and transmittance of nano ZnO (fresh & annealed), which recorded according to the wavelength range (200–2500 nm) are shown in Fig. 4a,b and Fig. 5a, b respectively. From Fig. 4a, b it is evident that ZnO films improve their optical absorption with increase of film thickness and with the annealing temperature. The absorbance curve exhibits weak absorption values with the increase in the wavelength ($\lambda > 500$ nm) which indicates the high transparency (T more than 90%) of the ZnO (fresh & annealed) films in this range of the wavelength (500–2500 nm) as shown in Fig. 5a,

Fig. 4 Optical absorbance for ZnO **a** fresh and **b** annealed (400 °C, 3 h) thin films
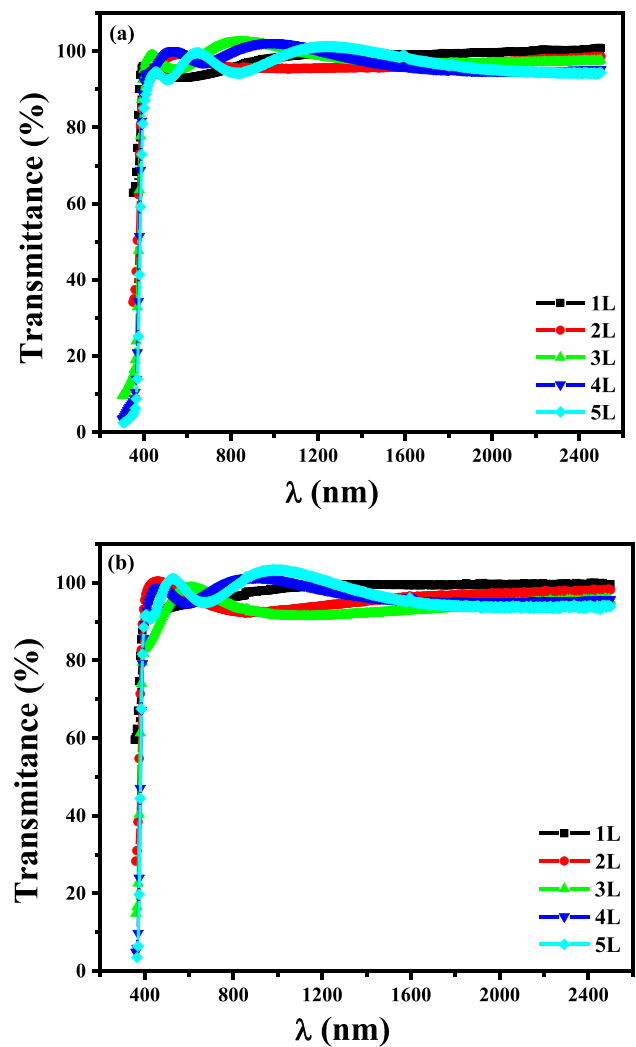
Fig. 5 Optical transmittance ZnO **a** fresh and **b** annealed (400 °C, 3 h) thin films

b. But, in the UV range, the absorbance curve suffers from a dramatic increase in its values due to the absorption of incident photons and the excitation of the electrons from the valence band to the conduction band at the absorption edges (at $\lambda \approx 400$ nm) for the ZnO films. We notice also from Fig. 5a, b, whereas the optical transmittance of 1L ZnO film (fresh & annealed) begins at around 60%, the transmittance of ZnO (4L & 5L) can begin from zero. This means that the increase in film thickness improves the transmittance of ZnO films in the wavelength range from 400 to 2500 nm and also it makes the absorbance takes the maximum values in the UV range ($\lambda < 400$ nm) as we note in Fig. 4a, b and Fig. 5a, b. From this result, we can conclude that the large thickness (4L & 5L). ZnO films are suitable to be used as pass filters where they can completely absorb and eliminate the UV photons from the passing light.

The absorption coefficient $\alpha(\lambda)$ and refractive index $n(\lambda)$ of the thin films under study can be evaluated via the Swanepoel manner [32], which depends on the transmittance interference fringes [33, 34]. The refractive index provides us information about the electronic polarization, local fields, and phase velocity of light propagating in the material. The refractive index $n(\lambda)$ in the transparent region where $\alpha \approx 0$ can be calculated according to the geometric mean (T_α) of T_M and T_m (maximum and minimum transmittances), as follow:

$$T_\alpha = \left(T_M \times T_m\right)^{1/2} \tag{4}$$

To get the refractive index, we use the following relation:

$$n = \left[H + \left(H^2 - n_S^2\right)^{1/2}\right]^{1/2}, \tag{5}$$

where $H = \dfrac{4n_S^2}{(n_s+1)T_\alpha^2} + \dfrac{n_S^2+1}{2}$

and the refractive index of the glass substrate is $n_s = 1.5$.

A feature, like a two-term Cauchy dispersion relationship, can be applied through the extrapolation of $n(\lambda)$ to short λ for all ZnO thin films as follows [32]:

$$n(\lambda) = a + \frac{b}{\lambda^2}, \tag{6}$$

Figure 6a, b refer to the spectral distribution of the refractive index of ZnO (fresh & annealed) thin films with various thicknesses. It is evident from that figure, the refractive index decreases, as a normal dispersion behavior with the increase of the wavelength of the incident photon. Furthermore, the behavior of n as a normal dispersion improves with the film thickness and with the annealing and takes the optimum values and behavior for ZnO (4L & 5L) films.

If n_1 and n_2 refer to the refractive indices that match the next two maxima λ_1 and λ_2 wavelengths, then the following relation can be used to calculate film thickness (d).
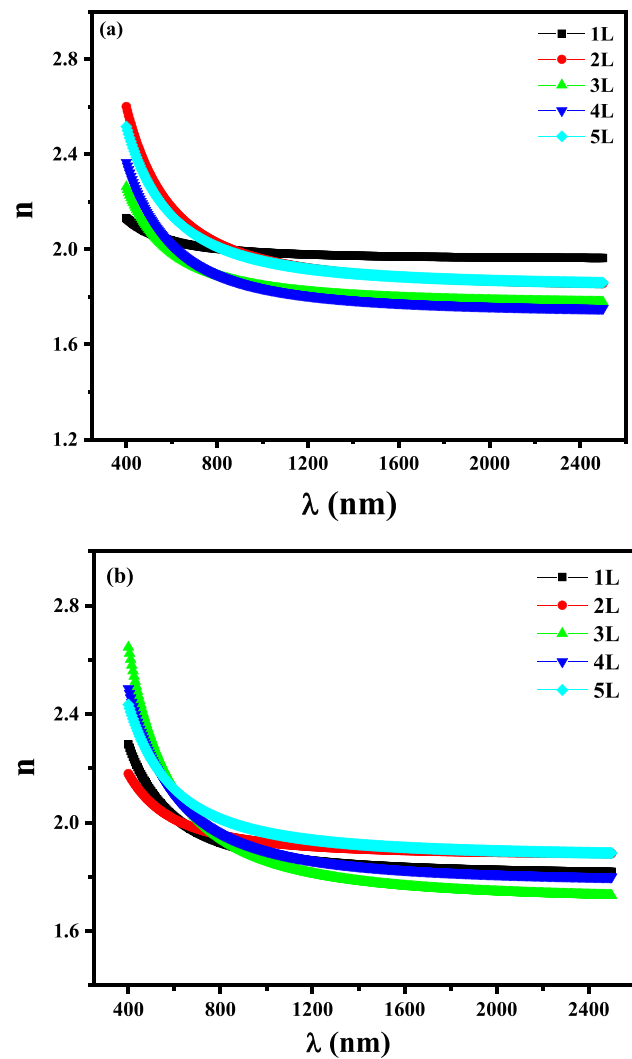

Fig. 6 Variation of refractive index, n, as a function of wavelength for ZnO **a** fresh and **b** annealed (400 °C, 3 h) thin films

$$d = \frac{\lambda_1 \times \lambda_2}{2\left(\lambda_1 n_2 - \lambda_1 n_1\right)} \tag{7}$$

Table 5 displays the values of the film thickness (d) for all of ZnO fresh and annealed thin films.

The absorption coefficient $\alpha(\lambda)$ of the studied films has been estimated by using the obtained values of n and d as follow:

$$\alpha = \frac{1}{d}\ln\left(\frac{1}{x}\right), \tag{8}$$

where the absorbance x is given by the formula [35]

$$x = \frac{P + \left[P^2 + 2QT_\alpha\left(1 - R_2R_3\right)\right]^{\frac{1}{2}}}{Q}, \tag{9}$$

where $P = \left(R_1 - 1\right)\left(R_2 - 1\right)\left(R_3 - 1\right)$
and $Q = 2T_\alpha\left(R_1R_2 + R_1R_3 - 2R_1R_2R_3\right)$

Table 5 Film thickness (*d*), optical band gap (E_g^{opt}), and dispersion parameters (E_0, E_d) for ZnO (fresh & annealed) thin films

ZnO	Fresh				400 °C, 3 h			
	d (nm)	E_g^{opt} (eV)	E_0 (eV)	E_d (eV)	*d* (nm)	E_g^{opt} (eV)	E_0 (eV)	E_d (eV)
1L	137	3.202	7.19	20.77	113	3.165	4.93	12.75
2L	152	3.196	4.47	13.62	140	3.220	5.74	15.33
3L	189	3.218	4.82	11.81	170	3.235	4.36	11.39
4L	260	3.218	4.52	11.22	182	3.238	4.46	12.28
5L	285	3.218	4.54	13.18	216	3.239	4.79	13.87

The reflectance of air-film R_1, film-substrate R_2, and substrate-air interfaces R_3, is given by:

$$R_1 = \left[\frac{1-n}{1+n}\right]^2, R_2 = \left[\frac{n-n_s}{n+n_s}\right]^2 \text{ and } R_3 = \left[\frac{n_s-1}{n_s+1}\right]^2$$

Figure 7a, b represent the absorption coefficient $\alpha(\lambda)$ vs. $h\upsilon$ for ZnO (fresh & annealed) thin films, respectively. As observed from that figure, the absorption coefficient increases with the increase of photon energy, and it is dramatically increased at the absorption edge of the films.
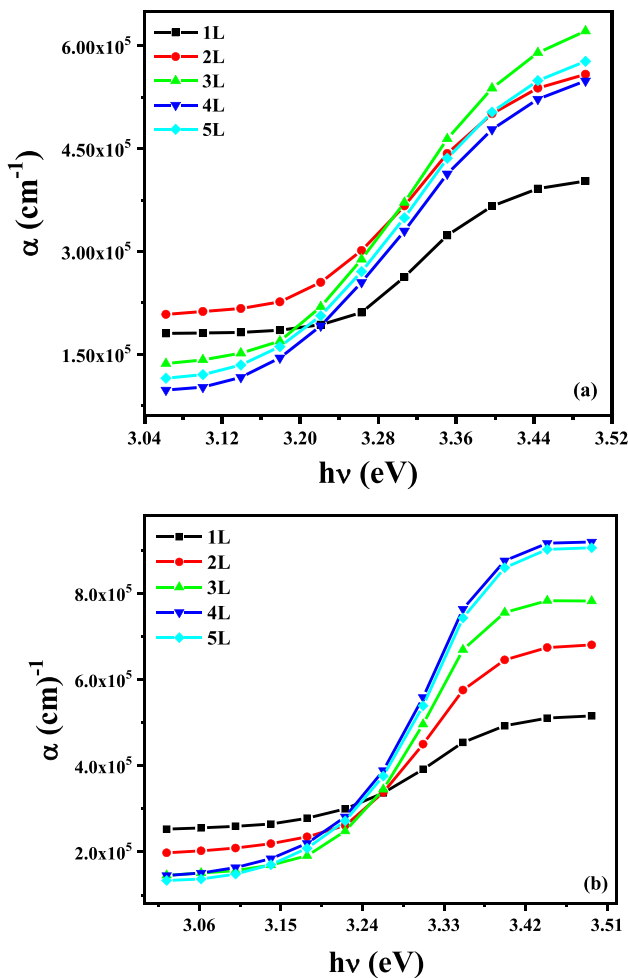
Fig. 7 Variation of absorption coefficient, α, as a function of photon energy for ZnO **a** fresh and **b** annealed (400 °C, 3 h) thin films

Furthermore, with the increase of the film thickness and annealing temperature, the absorption coefficient of the transparent ZnO films increases in the UV range and decreases in the Vis–NIR range due to the improvement of the crystal structure and the degradation of the defect states, where the localized defect states act as electron traps in the forbidden band gap for the photoexcited electrons.

The optical band gap E_g^{opt} can be determined through the elevated absorption region where $\alpha > 10^4$ cm^{-1}, from the well-known Tauc relation as follows [36, 37]:

$$\alpha h\upsilon = A\left(h\upsilon - E_g^{opt}\right)^n,$$
(10)

where *A* is a constant and *n* is the parameter which can determine the optical transition type. It takes the values of *1/2* as a direct allowed transition and *3/2* as a direct forbidden transition. The values of $(\alpha h\upsilon)^2$, (where $n = 1/2$) vs. $h\upsilon$ for the ZnO (fresh & annealed) thin films were plotted in Fig. 8a, b, respectively. The straight-line part of those curves at the absorption edges can be linearly fitted to obtain the direct optical band gap (E_g^{opt}) for all ZnO thin films under study. Table 5 shows E_g^{opt}'s values for ZnO (fresh & annealed) thin films of distinct thicknesses. The values of the optical band gap E_g^{opt} as illustrated in that table slightly change with the increase of the thickness and heat treatment. This effect may be due to the improvement of the crystal structure and the decrease of the defect density, and also the homogeneity improvement of the films with the thickness and heat treatment as shown in Tables 1, 2, 3, and 4.

The single oscillator energy E_0 and the dispersion energy E_d which relates to the optical conductivity and optical transition strength can be obtained through the single oscillator model proposed by Wemple–DiDomenico (WDD) where the refractive index in the transparent range can be written as follows [38, 39]:

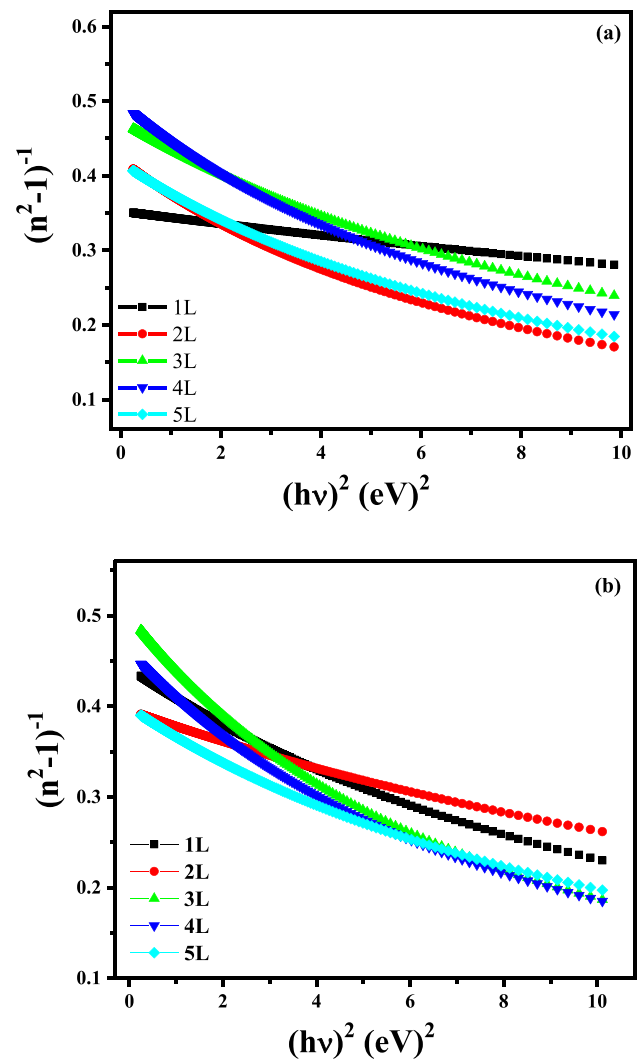$$n^2(h\upsilon) = 1 + \frac{E_0 E_d}{E_0^2 - (h\upsilon)^2},$$
(11)

By plotting $(n^2-1)^{-1}$ vs. $(h\upsilon)^2$ as shown in Fig. 9a, b. The intercept (E_0/E_d) and the slope ($E_0 E_d$)$^{-1}$ can be used
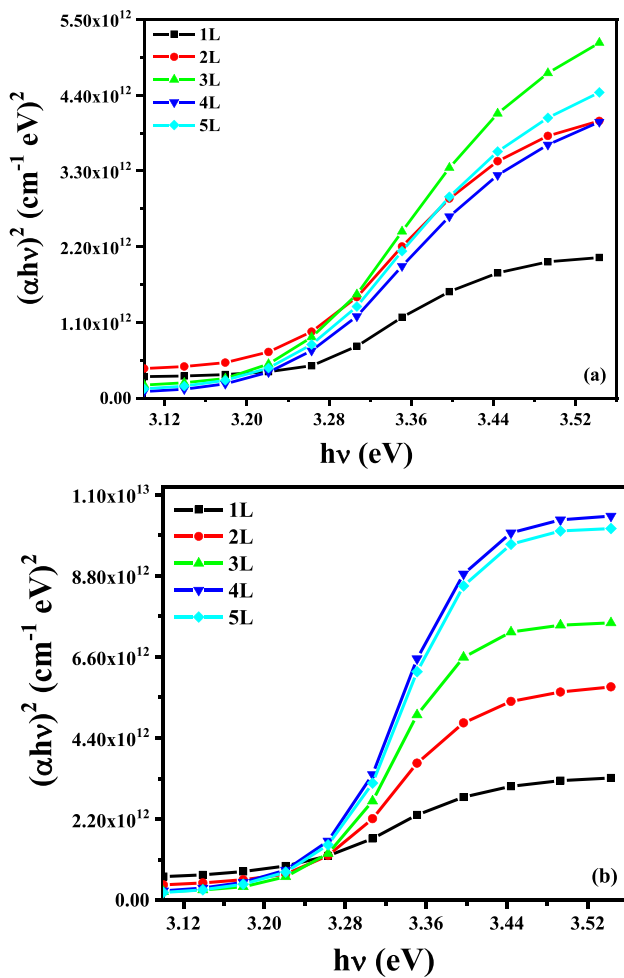
Fig. 8 Variation of $(\alpha h\nu)^2$ as a function of photon energy for ZnO **a** fresh and **b** annealed (400 °C, 3 h) thin films

Fig. 9 Variation of $(n^2-1)^{-1}$ versus $(h\nu)^2$ for ZnO **a** fresh and **b** annealed (400 °C, 3 h) thin films

to calculate the dispersion parameters E_0 and E_d. Table 5 demonstrates the values of the dispersion parameters E_0 and E_d for ZnO fresh and annealed thin films. As shown in that table, the values of the dispersion energy E_d slightly change with the film thickness and annealing temperature where it depends on the chemical bonds and bond energy in a material. Also, the change in the oscillator energy E_0 relates to the changes in the optical band values which exhibit small variation with the film thickness and annealing temperature according to the small changes in the crystallinity.

Optical conductivity of a material can be identified as the conductivity of the material due to the absorption of the incident photons. In the semiconductor materials, the conductivity increases with the incident photons due to the excitation of electrons from the valance band to the conduction band through the absorbed photons energy. Optical conductivity σ_{opt} can be evaluated through the absorption coefficient α as follows [40]:

$$\sigma_{opt} = \frac{\alpha n c}{4\pi}, \tag{12}$$

The refractive index is n, and the speed of light is c. Figure 10a, b show the change of optical conductivity σ_{opt} as a function of photon energy $h\nu$. It is apparent that with growing of photon energy, optical conductivity increases significantly, as electrons excitement through absorbing photon energy for fresh and annealed ZnO films [41, 42]. Furthermore, with the increase of film thickness and heat treatment the optical conductivity increases. This may be due to the improvement of crystal structure and degradation of the defect density. As the density of defects, which represents the recombination centers for the optically released electrons decreases with increase of film thickness and annealing temperature the σ_{opt} increases.
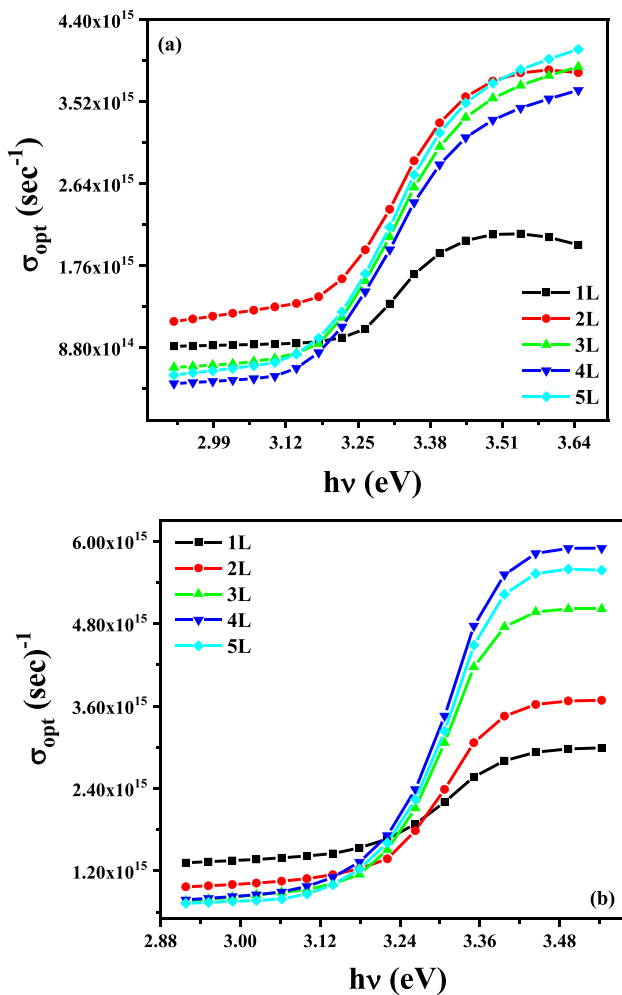
Fig. 10 Variation of optical conductivity σ_{opt} as a function of photon energy $h\nu$ for ZnO **a** fresh and **b** annealed (400 °C, 3 h) thin films

Photocatalytic activity of nanostructured ZnO thin films

The obtained optical results of the nanostructured ZnO (fresh & annealed) thin films directly indicate the applicability of these films in photocatalytic applications as efficient photocatalysts, especially in the UV range. ZnO (fresh & annealed) thin films were used for RO96 photodegradation at $\lambda = 254$ nm where they can fully absorb the incident photons and liberate the maximum number of the electrons in the UV range as explained in the optical section. The absorption spectrum of RO96 solution was obtained according to the illumination interval of time in order to monitor the degradation process of the RO96 dye in water. The RO96 concentration has been determined through the absorption spectra of the degraded RO96 solution using a quartz cell, obeying Beer–Lambert's law. The kinetics data of the reaction has been achieved via plotting of the normal concentration logarithm against the time interval of exposure. The initial concentration of the dye (RO96) aqueous solution is C_o and the concentration at time interval t is C. Therefore, the graph of ($ln(C/C_o)$) versus the illumination interval of time t is linear with a constant rate of k [43]. This relationship can be expressed according to the Langmuir–Hinshelwood (LH) model as follows [44]:

$$ln\left(C_0/C\right) = kt, \tag{13}$$

Figure 11a shows the relation between ($ln(C/C_o)$) versus the time t for ZnO fresh thin films with distinct thicknesses. The slopes of these fitted lines represent the values of the constant rate or reaction rate k min^{-1}. Figure 11b explains the thickness dependence of the constant rate k for ZnO fresh thin films. As we observe, Fig. 11a, b indicate a decrease of RO96 concentrations for all ZnO films, indicating a photocatalytic degradation of RO96 by ZnO thin films and the photocatalytic activity of ZnO films increases with thickness. Figure 12a, b show the photodegradation curves of RO96 using ZnO annealed (400 °C, 3 h) thin films with different thicknesses. It is noticed from that figure, there is an increase in the rate of degradation compared with that of the ZnO fresh films. This may be due to the improvement of the crystallinity for the annealed films, which can be associated with a decrease in the defect density as a recombination center for the photogenerated electron–hole pairs and hence the improvement of the optical absorption of the deposited films in the UV range with the thickness as described in optical section. In previous research, the reduction in the crystalline defects with the heat treatment increases the photocatalytic activity due to the lower rate of electron–hole recombination at the defect centers [45]. Furthermore, it is noted that the photodegradation efficiency of ZnO film rises as the number of layers (film thickness) increases to the four layers and reduces as the number of layers increased to 5L. The photodegradation efficiency of ZnO films takes the maximum value with the 4L ZnO fresh and annealed thin films, these findings have been clarified depending on the stoichiometry property of the ZnO thin film and the improvement of the optical absorbance with the film thickness and heat treatment. As shown in Table 3, the ZnO films with 4L of a thickness (fresh & annealed) have the stoichiometric ratios of Zn and O. So that, the ZnO films (fresh & annealed) of thickness 4L have the optimal thickness associated with the maximum photodegradation efficiency of RO96.

The degradation efficiency *(% degradation)* of the fresh and annealed different thickness films can be estimated as the following [10]:

$$\% \; D egradation = \left(1 - \frac{c}{c_0}\right) \times 100, \tag{14}$$

Figures 11c and 12c show the *% degradation* against the UV irradiation time, t for fresh and annealed films,

Fig. 11 Photodegradation curves of RO96 using ZnO fresh thin films as photo-catalysts **a** $ln(C/C_o)$ versus t, **b** constant rate k versus no. of layers (film thickness), and **c** %degradation efficiency against UV irradiation time, t
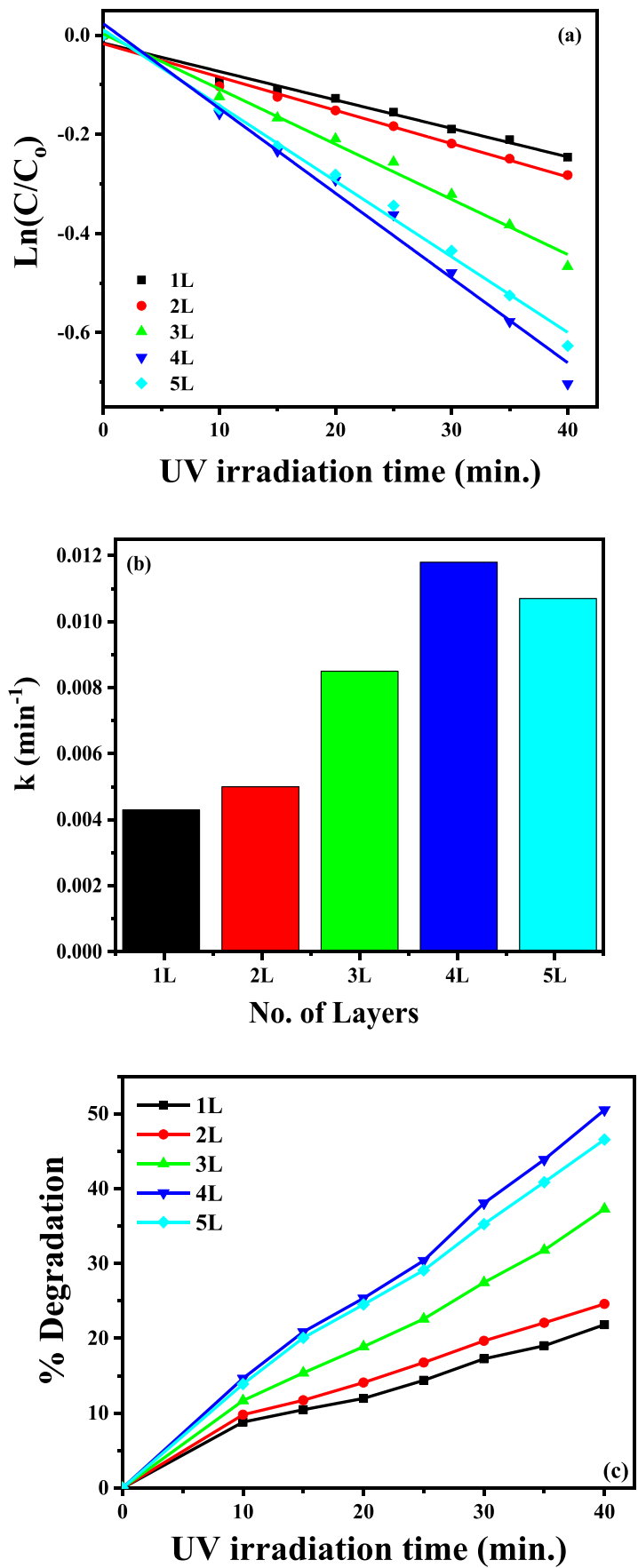
Fig. 12 Photodegradation curves of RO96 using ZnO annealed (400 °C, 3 h) thin films as photocatalysts **a** $ln(C/C_o)$ versus t, **b** constant rate k versus no. of layers (film thickness), and **c** %degradation efficiency against UV irradiation time, t
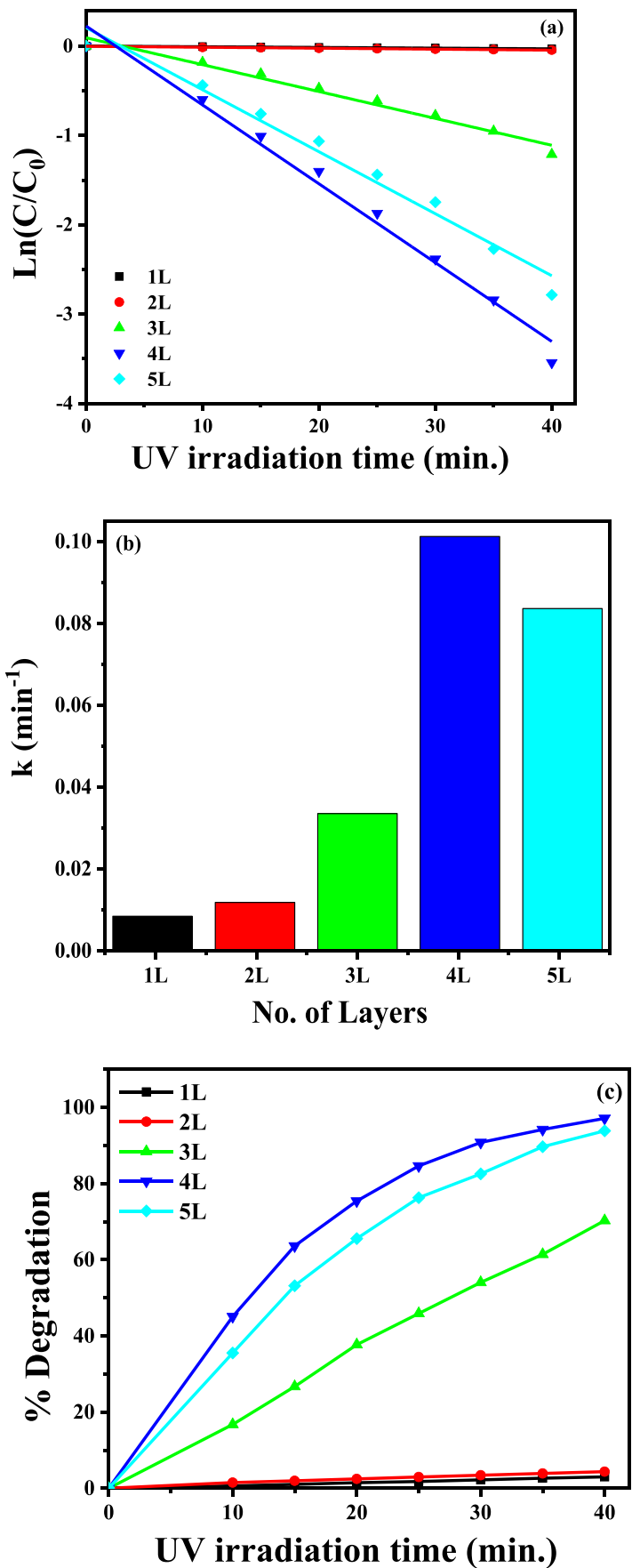
respectively. As shown in Fig. 11c, the % *degradation* increases with the film thickness and takes the maximum value (% *degradation = 50.5*) at 4L of thickness. With the heat treatment at 400 °C for 3 h, the crystal structure and the stoichiometry of the films observably improved as explained in Tables 3 and 4. So the % *degradation* of the annealed films dramatically increased as shown in Fig. 12c in comparison with that of the fresh films. It reaches 97.11% for 4L (400 °C) film as a maximum value. It can be explained according to the improvement in the crystal structure and the stoichiometric composition of the 4L (400 °C) film as shown in Tables 3 and 4. For practical applications, both the stability and recyclability of photocatalysts are highly essential. So according to the findings of UV-induced photocatalytic activity of 4L ZnO annealed (400 °C, 3 h) thin film in RO96 photodegradation the cycling experiments can be proceeded to prove the stability of ZnO films as efficient photocatalysts in the UV range. Figure 13 displays the cycling experiments for 4L ZnO annealed (400 °C, 3 h) thin film under UV irradiation. As observed from that figure, there is no significant loss in the photocatalytic activity after 5 cycles of reusing for ZnO (4L, 400 °C) as strong evidence for the high stability for reusing of the nanostructured ZnO thin films as photocatalysts. Table 6 shows the photocatalytic parameters of ZnO films as in the present work and also of ZnO nanoparticles from different previous researches [10, 46–52]. As shown in Table 6, ZnO film in the present work has the highest value of the photodegradation efficiency (97.11%) for the RO96 in the shortest period of irradiation time about 40 min with the highest rate of degradation 0.1012 min^{-1} compared with the previous works. The high photodegradation efficiency of our ZnO film as a photocatalyst indicates that our ZnO film
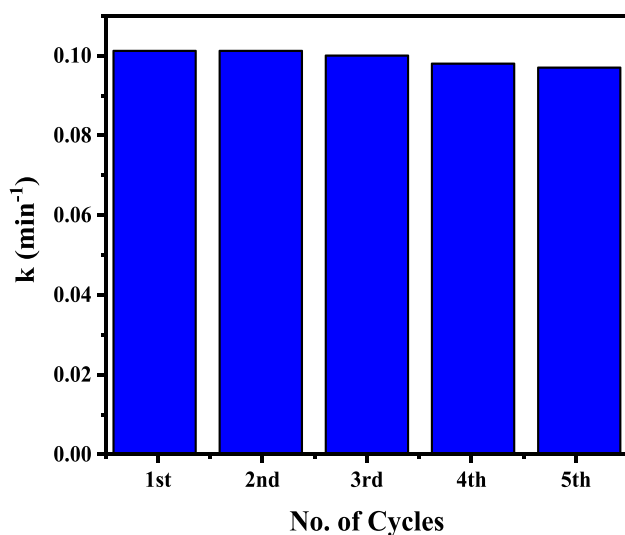
Fig. 13 Cycling experiments for 4L ZnO annealed (400 °C, 3 h) thin film

which was deposited by the sol–gel spin-coating method and annealed at 400 °C for 3 h has the optimum thickness as a photocatalyst film. The obtained results assure the applicability of ZnO film (4L, 400 °C) as a high efficiency and stability photocatalyst thin film in photocatalytic applications. From these results, we can conclude that our films which were deposited by the sol–gel spin-coating technique and annealed at 400 °C for 3 h have the optimum thickness and overpass the other samples from the previous works as efficient photocatalysts for water purification from the organic dyes.

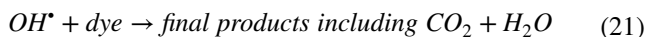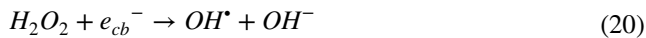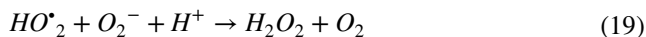## Photocatalytic mechanism of nanostructured ZnO thin films

Figure 14 shows the schematic diagram for the photodegradation mechanism of RO96 dye by ZnO thin film as a photocatalyst. The photocatalytic activity of ZnO thin film mainly depends on the photogenerated electron–hole pairs by the UV illumination. Where the conduction band electrons (e_{cb}^{-}) and valence band holes (h_{vb}^{+}) are generated on the surfaces of ZnO thin films when they are illuminated by UV light with energy ($h\upsilon$) exceeding or equaling to its band gap energy as follows:

$$ZnO + h\upsilon \rightarrow e_{cb}^{-} + h_{vb}^{+} \tag{15}$$

Holes can react with water molecule adhering to the surfaces of ZnO thin films to form highly reactive hydroxyl radicals ($OH^{\bullet}$) as follows:

$$H_2O + h_{vb}^{+} \rightarrow OH^{\bullet} + H^{+} \tag{16}$$

However, oxygen molecule on the surface of ZnO thin films is reduced by a conduction band electron to superoxide. After a sequence of reactions, further productions of hydroxyl radicals ($OH^{\bullet}$) can be provided. The formed radicals have a powerful oxidation ability to degrade the organic dye as described below:

$$O_2 + e_{cb}^{-} \rightarrow O_2^{-} \tag{17}$$

$$O_2^{-} + H^{+} \rightarrow HO_2^{\bullet} \tag{18}$$

$$HO_2^{\bullet} + O_2^{-} + H^{+} \rightarrow H_2O_2 + O_2 \tag{19}$$

$$H_2O_2 + e_{cb}^{-} \rightarrow OH^{\bullet} + OH^{-} \tag{20}$$

$$OH^{\bullet} + dye \rightarrow final\ products\ including\ CO_2 + H_2O \tag{21}$$

The photocatalytic efficiency of ZnO thin films in the decomposition of RO96 with aqueous solutions can be described on the base of the mean grain size, surface roughness, and the presence of oxygen vacancies and

Table 6 Photocatalytic parameters of ZnO film and ZnO nanoparticles from different references and ZnO film from the present work

Catalyst	Prep. method	Thickness (nm)	Annealing Temp. (°C)	Band gap (eV)	Dye	k (min^{-1})	Irrad. time	%Degrad	Ref
ZnO	Sol–gel spin coating	182	400	3.238	RO96	0.1012	40 min	97.11	Present work
ZnO	Spray pyrol	200	400	3.283	Phenol	0.01419	40 min	40.13	[10]
ZnO	Sol–gel	NPs	700	3.120	RhB	0.0180	120 min	91.41	[46]
ZnO	Eco-friendly green route	NPs	-	3.370	MB	-	540 min	96	[47]
ZnO	co-precip	NPs	450	3.90	MO	-	150 min	≈ 40	[48]
ZnO	Pulse laser deposit	film	25	3.250	RhB		6 h	91%	[49]
ZnO	Sol–gel	NPs	550	-	MB		15 min	65.5	[50]
ZnO	RF sputter	film	25	3.350	MB	0.0078	3 h	≈ 80	[51]
ZnO	Sol–gel dip-coat	film	350	3.360	MB	00,032	5 h	55	[52]
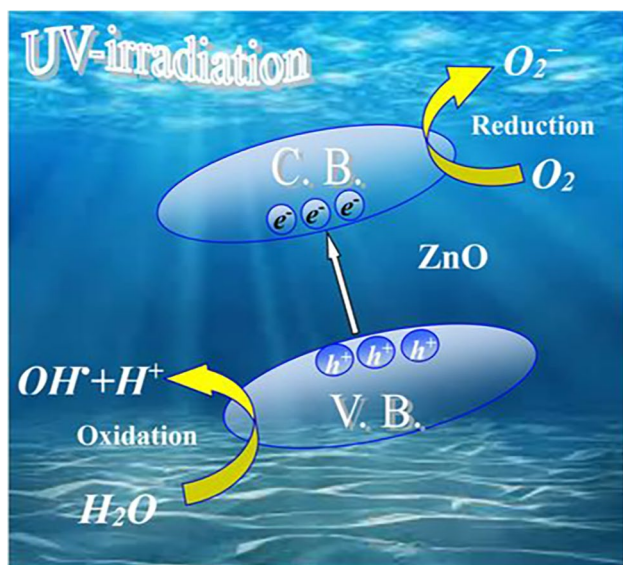
Fig. 14 Schematic diagram for the photocatalytic mechanism of ZnO thin films

interstitial oxygen defects. Surface defects were suitable for electrons or holes trapping, as they are related to the oxygen vacancy. This reduces the likelihood of recombination and eventual redox reactions can take place. As stated, vacancies in oxygen play a significant part in the decomposition of the organic dye under UV light irradiation. They create empty ZnO energy levels between conduction band (*C.B.*) and valence band (*V.B.*), which behave like deep defect donors close to *VB*'s top [53]. However, the oxygen vacancies and interstitial oxygen defects can enhance the electron–hole pair separation rate in ZnO thin films, so it can be considered as the active sites of the ZnO photocatalyst. The photocatalytic mechanism of nanostructured ZnO has been explained in a lot of reports as shown in refs [54, 55].

Conclusion

Nanostructured thin films of ZnO can be synthesized at room temperature with a non-vacuum sol–gel spin-coating technique. The films acquired are transparent, uniform, well smooth, and without macroscopic defects. The XRD and AFM studies have confirmed the nanocrystalline structure of the deposited ZnO thin films. The crystallites in the ZnO films have a preferred orientation along (002) plane according to the hexagonal wurtzite structure. The energy-dispersive X-ray technique has shown that with the annealing temperature the oxygen ratio in ZnO films rises. By heat treatment at 400 °C for 3 h and increase of film thickness, the crystal structure of ZnO thin films has been improved, and also the homogeneity and optical absorbance have been enhanced. ZnO thin films have a direct optical band gap determined by the Tauc procedure. By using the Wemple–DiDomenico single-effect oscillator model, the dispersion parameters E_0 and E_d have been identified. The values of the optical band gaps and optical transmittance confirm the applicability of the ZnO films as efficient films in different optoelectronic applications. The ZnO films (fresh & annealed) of thickness 4L have the optimal thickness associated with the maximum photodegradation efficiency of RO96. The annealed (400 °C, 3 h) ZnO film with 4L of thickness has the maximum degradation efficiency and the highest photodegradation constant rate for water purification from RO96 also it has high stability for reusing as optimal photocatalyst in photocatalytic applications.

Declarations

Competing interests The authors declare no competing interests.

References

1. Edinger, S., Bansal, N., Bauch, M., Wibowo, R.A., Ujvari, G., Hamid, R., Trimmel, G., Dimopoulos, T.: Highly transparent and conductive indium-doped zinc oxide films deposited at low substrate temperature by spray pyrolysis from water-based solutions. J. Mater. Sci. **52**, 8591–8602 (2017)

2. Deepa Rani, T., Ramamurthi, K., Leela, S.: Structural and optical properties of Gd doped ZnO thin films by spray pyrolysis technique. AIP. Conf. Proc. **2117**, 020003 (2019). https://doi.org/10.1063/1.5114583

3. Chen, Y.-C., Li, Y.-J., Hsu, Y.-K.: Enhanced performance of ZnO-based dye-sensitized solar cells by glucose treatment. J. Alloy. Compd. **748**, 382–389 (2018). https://doi.org/10.1016/j.jallcom.2018.03.189

4. Vittal, R., Ho, K.-C.: Zinc oxide based dye-sensitized solar cells: a review. Renew. Sustain. Energy Rev. **70**, 920–935 (2017). https://doi.org/10.1016/j.rser.2016.11.273

5. Muchuweni, E., Sathiaraj, T.S., Nyakotyo, H.: Synthesis and characterization of zinc oxide thin films for optoelectronic applications. Heliyon **3**(4), e00285 (2017). https://doi.org/10.1016/j.heliyon.2017.e00285

6. Liu, H., Liu, Y.-F., Xiong, P.-P., Chen, P., Li, H.-Y., Hou, J.-W., Bo-Nan Kang, Yu., Duan,: Aluminum-doped zinc oxide transparent electrode prepared by atomic layer deposition for organic light emitting devices. IEEE Trans. Nanotechnol. **16**(4), 634–638 (2017). https://doi.org/10.1109/TNANO.2017.2700408

7. Agarwala, S., Raib, P.: Eric Navarrete Gatell, Eduard Llobet, Frank Güell, Manoj Kumar, Kamlendra Awasthi, Gas sensing properties of ZnO nanostructures (flowers/rods) synthesized by hydrothermal method. Sens. Actuators, B Chem. **292**, 24–31 (2019). https://doi.org/10.1016/j.snb.2019.04.083

8. Chava, R.K., Kang, M.: Improving the photovoltaic conversion efficiency of ZnO based dye sensitized solar cells by indium doping. J. Alloy. Compd. **692**, 67–76 (2017). https://doi.org/10.1016/j.jallcom.2016.09.029

9. Sujinnapram, S., Moungsrijun, S.: Additive SnO2-ZnO composite photoanode for improvement of power conversion efficiency in dye-sensitized solar cell. Procedia Manufacturing **2**, 108–112 (2015). https://doi.org/10.1016/j.promfg.2015.07.019

10. Abdel-Galil, A., Mai Hussien, S.A., Yahia, I.S.: Synthesis and optical analysis of nanostructured F-doped ZnO thin films by spray pyrolysis: transparent electrode for photocatalytic applications. Optical Mater. **114**, 110894 (2021). https://doi.org/10.1016/j.optmat.2021.110894

11. Deak, G.: Florina Diana Dumitru, Mihaela Andreea Moncea, Ana Maria Panait, Andreea Georgiana Baraitaru, Marius Viorel Olteanu, Madalina Georgiana Boboc, Silvius Stanciu, Synthesis of Zno nanoparticles for water treatment applications. Int. J. Conserv. Sci. **10**(2), 343–350 (2019)

12. Grivel, J.-C.: Photocatalytic Water Purification with ZnO Thin Films in Demineralized as Well as Natural Waters. Physica Status Solidi A **216**(14), 1800880 (2019). https://doi.org/10.1002/pssa.201800880

13. Vallejo, W., Cantillo, A., Díaz-Uribe, C.: Methylene blue photodegradation under visible irradiation on Ag-Doped ZnO thin films. Int J Photoenergy **2020**(1627498), 11 (2020). https://doi.org/10.1155/2020/1627498

14. Nagaraja, R., Kottam, N., Girija, C.R., Nagabhushana, B.M.: Photocatalytic degradation of Rhodamine B dye under UV/solar light using ZnO nanopowder synthesized by solution combustion route. Powder Technol. **215–216**, 91–97 (2012). https://doi.org/10.1016/j.powtec.2011.09.014

15. Bosi Yin, Siwen Zhang, Dawei Zhang, Yang Jiao, Yang Liu, Fengyu Qu, Xiang Wu, ZnO Film photocatalysts. J. Nanomater. **2014**, 7. Article ID 186916, https://doi.org/10.1155/2014/186916

16. Korake, P.V., Kadam, A.N., Garadkar, K.M.: Photocatalytic activity of Eu^{3+}-doped ZnO nanorods synthesized via microwave assisted technique. J. Rare Earths **32**(4), 306–313 (2014). https://doi.org/10.1016/s1002-0721(14)60072-7

17. Zhang, X., Qin, J., Xue, Y., Yu, P., Zhang, B., Wang, L., Liu, R.: Effect of aspect ratio and surface defects on the photocatalytic activity of ZnO nanorods. Sci Rep **4**, 4596 (2014). https://doi.org/10.1038/srep04596

18. El-Shazly, A.N., Rashad, M.M., Abdel-Aal, E.A., Ibrahim, I.A., El-Shahat, M.F., Shalan, A.E.: Nanostructured ZnO photocatalysts prepared via surfactant assisted co-precipitation method achieving enhanced photocatalytic activity for the degradation of methylene blue dyes. J. Environ. Chem. Eng. **4**, 3177–3184 (2016). https://doi.org/10.1016/j.jece.2016.06.018

19. Alfaro Cruz, M.R., Ceballos-Sanchez, O., Luévano-Hipólito, E., Torres-Martínez, L.M.: ZnO thin films deposited by RF magnetron sputtering: Effects of the annealing and atmosphere conditions on the photocatalytic hydrogen production. Int. J. Hydrogen Energy **43**(22), 10301–10310 (2018). https://doi.org/10.1016/j.ijhydene.2018.04.054

20. Opel, M., Geprägs, S., Althammer, M., Brenninger, T., Gross, R.: Laser molecular beam epitaxy of ZnO thin films and heterostructures. J. Phys. D Appl. Phys. **47**(3), 034002 (2013). https://doi.org/10.1088/0022-3727/47/3/034002

21. Akinwunmi, O.O., Ogundeji, J.A.O., Famojuro, A.T., Akinwumi, O.A., Ilori, O.O., Fadodun, O.G., Ajayi, E.O.B.: Preparation and some properties of metal organic chemical vapour deposited Al-doped ZnO thin films using single solid precursors. J. Mod. Phys. **9**, 2073–2089 (2018)

22. Wisz, G., Virt, I., Sagan, P., Potera, P., Yavorskyi, R.: Structural, Optical and electrical properties of zinc oxide layers produced by pulsed laser deposition method. Nanoscale Res. Lett. **12**, 253 (2017). https://doi.org/10.1186/s11671-017-2033-9

23. Cho, J., Hwang, S., Ko, D.-H., Chung, S.: Transparent ZnO thin-film deposition by spray pyrolysis for high-performance metal-oxide field-effect transistors. Material **12**, 3423 (2019). https://doi.org/10.3390/ma12203423

24. Mata, V., Maldonado, A., de la Luz Olvera, M.: Deposition of ZnO thin films by ultrasonic spray pyrolysis technique. Effect of the milling speed and time and its application in photocatalysis. Mater. Sci. Semicond. Process. **75**, 288–295 (2018). https://doi.org/10.1016/j.mssp.2017.11.038

25. Tugral Arslan, H., Urper, O., Ozdurmusoglu, T., Arslan, C., Baydogan, N.: Optical model of sol-gel derived Al: ZnO thin film. Acta Scientific Ophthalmology **2**(10), 12–15 (2019)

26. Arif, M., Sanger, A., Vilarinho, P.M., Singh, A.: Effect of annealing temperature on structural and optical properties of sol–gel-derived ZnO thin films. J. Electron. Mater. **47**, 7 (2018). https://doi.org/10.1007/s11664-018-6217-6

27. Efkere, H.I., Tataroglu, A., Cetin, S.S., Topaloglu, N., Gonullu, M.P., Ates, H.: The effect of thickness on the optical, structural and electrical properties of ZnO thin film deposited on n-type Si. J. Mol. Struct. **1165**, 376–380 (2018). https://doi.org/10.1016/j.molstruc.2018.04.022

28. Kumar, V., Singh, N., Mehra, R.M., Kapoor, A., Purohit, L.P., Swart, H.C.: Role of film thickness on the properties of ZnO thin films grown by sol-gel method. Thin Solid Films **539**, 161–165 (2013). https://doi.org/10.1016/j.tsf.2013.05.088

29. Abdel-Galil, A., Mai, S.A., Hussien, I.S., Yahia.: Low cost preparation technique for conductive and transparent Sb doped SnO_2 nanocrystalline thin films for solar cell applications. Superlattices and Microstructures **147**(2020), 106697. https://doi.org/10.1016/j.spmi.2020.106697

30. Ali, M.Y., Khan, M.K.R., Karim, A.M.M.T., Rahman, M.M., Kamruzzaman, M.: Effect of Ni doping on structure, morphology and opto-transport properties of spray pyrolised ZnO nanofiber. Heliyon **6**(3), e03588 (2020). https://doi.org/10.1016/j.heliyon.2020.e03588

31. Gürakar, S., Serin, T.: Comprehensive structural analysis and electrical properties of (Cu, Al and In)-doped SnO2 thin films. Mater. Sci. Eng., B **251**, 114445 (2019). https://doi.org/10.1016/j.mseb.2019.114445

32. Swanepoel, R.: Determination of the thickness and optical constants of amorphous silicon. J. Phys. E: Sci. Instrum. **16**, 1214 (1983). https://doi.org/10.1088/0022-3735/16/12/023

33. Manifacier, J.C., Gasiote, J., Fillard, J.P.: A simple method for the determination of the optical constants n, k and the thickness of a weakly absorbing thin film. J. Phys. E:Sci. Instrum. **9**, 1002 (1976)

34. Abdel-Galil, A., Moussa, N.L., Yahia, I.S.: Synthesis and optical characterization of nanocrystalline fluorine-doped tin oxide films: conductive window layer for optoelectronic applications. Appl. Phys. A **127**, 474 (2021). https://doi.org/10.1007/s00339-021-04632-4

35. Connell, G.A.N., Lewis, A.J.: Comments on the evidence for sharp and gradual optical absorption edges in amorphous germanium. Phys. Status Solidi B **60**, 291 (1973)

36. Tauc, J., Menth, A.: States in the gap. J. Non-Cryst. Solids **8–10**, 569–585 (1972)

37. Mott, N.F., Davis, E.A.: Electronic process in non-crystalline materials. Calendron Press, Oxford (1979)

38. DrDidomenico, M., Jr., Wemple, S.H.: Oxygen-octahedra ferroelectrics I Theory of electro-optical and nonlinear optical effects. J. App. Phys. **40**, 720 (1969)

39. Wemple, S.H., DiDomenico, M., Jr.: Behavior of the electronic dielectric constant in covalent and ionic materials. Phys. Rev. B **3**, 1338 (1971)

40. Pankove, J.I.: Optical processes in semiconductors, p. 91. Dover Publications Inc., New York (1975)

41. Sedky, A., Ali, A.M., Mohamed, M.: Structural and optical investigation of pure and Al doped ZnO annealed at different temperatures. Opt. Quant. Electron. **52**, 42 (2020). https://doi.org/10.1007/s11082-019-2158-4

42. Alsaad, A.M., Ahmad, A.A., Qattan, I.A., Al-Bataineh, Q.M., Albataineh, Z.: Structural, optoelectrical, linear, and nonlinear optical characterizations of dip-synthesized undoped ZnO and group III elements (B, Al, Ga, and In)-doped ZnO thin films. Crystals **10**, 252 (2020). https://doi.org/10.3390/cryst10040252

43. Islam, M.R., Rahman, M., Farhad, S.F.U., Podder, J.: Structural, optical and photocatalysis properties of sol–gel deposited Al doped ZnO thin films. Surf. Interfaces **16**, 120–126 (2019)

44. Alberici, R.M., Jardim, W.F.: Photocatalytic destruction of VOCs in the gas-phase using titanium dioxide. Appl. Catal. B **14**(1–2), 55–68 (1997). https://doi.org/10.1016/s0926-3373(97)00012-x

45. Torres-Hernández, J.R., Ramírez-Morales, E., Rojas-Blanco, L., Pantoja-Enriquez, J., Oskam, G., Paraguay-Delgado, F., Escobar-Morales, B., Acosta-Alejandro, M., Díaz-Flores, L.L., Pérez-Hernández, G.: Structural, optical and photocatalytic properties of ZnO nanoparticles modified with Cu. Mater. Sci. Semicond. Process. **37**, 87–92 (2015). https://doi.org/10.1016/j.mssp.2015.02.009

46. González-Crisostomo, J.C., López-Juárez, R., Petranovskii, V.: Photocatalytic degradation of rhodamine B dye in aqueous suspension by ZnO and M-ZnO (M = La^{3+}, Ce^{3+}, Pr^{3+} and Nd^{3+}) nanoparticles in the presence of UV/H_2O_2. Proc. **9**, 1736 (2021). https://doi.org/10.3390/pr9101736

47. Mirgane, N.A., Shivankar, V.S., Kotwal, S.B., Wadhawa, G.C., Sonawale, M.C.: Degradation of dyes using biologically synthesized zinc oxide Nanoparticles. Mater. Today: Proc. **37**, 849–853 (2021). https://doi.org/10.1016/j.matpr.2020.06.037

48. Senthil Kumar, M., Arunagiri, C.: Efficient photocatalytic degradation of organic dyes using Fe-doped ZnO nanoparticles. J Mater Sci: Mater Electron **32**, 17925–17935 (2021). https://doi.org/10.1007/s10854-021-06328-0

49. Yudasari, N., Kennedy, D.S., Suliyanti, M.M.: Pulse laser deposition (PLD) technique for ZnO photocatalyst fabrication. IOP Conf Series: J. Phys.: Conf Series **1191**, 012009 (2019). https://doi.org/10.1088/1742-6596/1191/1/012009

50. Zhu, X., Wang, J., Yang, D., Liu, J., He, L., Tang, M., Feng, W., Wu, X.: Fabrication, characterization and high photocatalytic activity of Ag–ZnO heterojunctions under UV-visible light. RSC Adv **11**, 27257 (2021). https://doi.org/10.1039/d1ra05060e

51. Khalfallah, B., Riahi, I., Chaabouni, F.: Structural, optical and electrical properties of Cu doped ZnO thin films grown by RF magnetron sputtering: application to solar photocatalysis. Opt. Quantum Electron. https://doi.org/10.21203/rs.3.rs-211058/v1

52. Islam, M.R., Azam, M.G.: Enhanced photocatalytic activity of Mg-doped ZnO thin films prepared by sol–gel method. Surf Eng. https://doi.org/10.1080/02670844.2020.1801143

53. Zhang, C., Geng, X., Liao, H., Li, C.J., Debliquy, M.: Room-temperature nitrogen-dioxide sensors based on ZnO_{1-x} coatings deposited by solution precursor plasma spray. Sens. Actuators B **242**, 102–111 (2017)

54. Ong, C.B., Ng, L.Y., Mohammad, A.W.: A review of ZnO nanoparticles as solar photocatalysts: synthesis, mechanisms and applications. Renew. Sustain. Energy Rev. **81**, 536–551 (2018). https://doi.org/10.1016/j.rser.2017.08.020

55. Mataa, V., Maldonado, A., de la Luz Olvera, M.: Deposition of ZnO thin films by ultrasonic spray pyrolysis technique. Effect of the milling speed and time and its application in photocatalysis. Mater. Sci. Semiconductor Proc. **75**, 288–295 (2018). https://doi.org/10.1016/j.mssp.2017.11.038